

Stability Analysis of Sharpness-Aware Minimization

Hoki Kim, Jinseong Park, Yujin Choi, and Jaewook Lee

Abstract—Sharpness-aware minimization (SAM) is a recently proposed training method that seeks to find flat minima in deep learning, resulting in state-of-the-art performance across various domains. Instead of minimizing the loss of the current weights, SAM minimizes the worst-case loss in its neighborhood in the parameter space. In this paper, we demonstrate that SAM dynamics can have convergence instability that occurs near a saddle point. Utilizing the qualitative theory of dynamical systems, we explain how SAM becomes stuck in the saddle point and then theoretically prove that the saddle point can become an attractor under SAM dynamics. Additionally, we show that this convergence instability can also occur in stochastic dynamical systems by establishing the diffusion of SAM. We prove that SAM diffusion is worse than that of vanilla gradient descent in terms of saddle point escape. Further, we demonstrate that often overlooked training tricks, momentum and batch-size, are important to mitigate the convergence instability and achieve high generalization performance. Our theoretical and empirical results are thoroughly verified through experiments on several well-known optimization problems and benchmark tasks.



1 INTRODUCTION

WITH a large number of parameters, deep learning models have shown remarkable improvements across a variety of domains. However, these over-parameterized deep learning models may suffer from poor generalization, even though they enjoy near zero training loss. To alleviate this overfitting problem, prior studies have suggested diverse techniques such as augmentation and regularization.

Recently, researchers have become interested in exploring the relationship between the geometric characteristics of the loss surface and the generalization performance [1], [2], [3]. Theoretical and empirical studies have demonstrated that the generalization performance is potentially related to the sharpness of the loss landscape and that an optimum with a flatter loss landscape can lead to better generalization. Based on these prior studies, Foret et al. [4] recently proposed a new training framework called *sharpness-aware minimization* (SAM) that substantially improves the generalization performance on various tasks [4], [5], [6]. The key idea of SAM is to minimize the maximum loss near its neighborhood in the weight space instead of minimizing the loss of the current weight. Thus, SAM can reach an optimum with a flatter loss landscape, resulting in improved generalization performance. Owing to its simplicity and ease of implementation, SAM has been adopted by many practitioners for training neural networks and improving the generalization performance.

However, we identify an instability in the convergence process of SAM dynamics near a saddle point, which may cause the suboptimal minimum problem. As shown in Figure 1, the Beale function, a widely used optimization

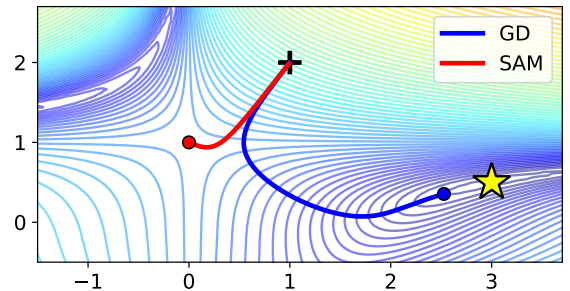


Fig. 1. The optimization has begun at the point indicated by the plus sign, and the global minimum is indicated by the yellow star. SAM appears to be stuck at the saddle point, rather than converging to the global minimum.

problem, is optimized using both vanilla gradient descent (GD) and SAM. GD reaches the global minimum (yellow star) but SAM is trapped in the saddle point. As deep learning models are highly non-linear and thus have multiple local minima and saddle points [7], [8], this convergence instability near a saddle point should be investigated.

To provide a comprehensive understanding of the convergence instability near a saddle point in SAM dynamics, we analyze the dynamics of SAM near saddle points from the viewpoint of a dynamical system and show that SAM may not converge due to its gradient oscillation. We then prove that saddle points can become attractors under certain circumstances. We extend our investigation to the utilization of stochastic optimization with mini-batch sampling and establish the property of SAM diffusion, demonstrating that SAM requires more time to escape saddle points than stochastic gradient descent (SGD). Based on the diffusion, we further identify the importance of often overlooked training tricks, momentum and batch size, on the convergence instability of SAM. To the best of our knowledge, this is the first work that identifies and investigates the convergence instability of SAM near a saddle point.

• H. Kim, J. Park, Y. Choi, and J. Lee are with the Department of Industrial Engineering, Seoul National University, 599 Gwanak-ro, Gwanak-gu, Seoul 151-744, South Korea.

Please address all correspondence to Dr. Jaewook Lee, Department of Industrial Engineering, Seoul National University, 1 Gwanak-ro, Gwanak-gu, Seoul 151-744, South Korea. E-mail address: jaewook@snu.ac.kr.

The main contributions of this study can be summarized as follows:

- We identify the convergence instability of SAM and theoretically prove the difficulty of escaping saddle points under SAM dynamics from the perspective of a dynamical system.
- We investigate the difficulty of saddle point escape under stochastic dynamical systems by establishing SAM diffusion and identify the importance of momentum and batch size for escaping saddle points with SAM diffusion.
- We conduct various experiments to support our theoretical results on a range of optimization settings, from a basic optimization problem to neural network-based benchmark tasks.

2 BACKGROUND

Given a loss function $\ell(\cdot)$ and weight parameters \mathbf{w} , the traditional optimization, the so-called empirical risk minimization, tries to minimize the following objective:

$$\min_{\mathbf{w}} \mathcal{L}(\mathbf{w}; \mathcal{S}) := \frac{1}{n} \sum_{(\mathbf{x}, \mathbf{y}) \in \mathcal{S}} \ell(\mathbf{w}; \mathbf{x}, \mathbf{y}), \quad (1)$$

where $\mathcal{S} = \{\mathbf{x}_i, \mathbf{y}_i\}_{i=1}^n$ is a sampled training dataset with n instances. Under the general i.i.d. assumption on data, (1) generally yields a feasible solution of \mathbf{w} on the true distribution of data \mathcal{D} ,

$$\min_{\mathbf{w}} \mathcal{L}(\mathbf{w}; \mathcal{D}) := \mathbb{E}_{(\mathbf{x}, \mathbf{y}) \sim \mathcal{D}} [\ell(\mathbf{w}; \mathbf{x}, \mathbf{y})]. \quad (2)$$

However, in common practice, the i.i.d assumption is often violated by the limitation of training data and model structure. Therefore, a *generalization gap* can be defined as

$$\mathcal{E}(\mathbf{w}) = \mathcal{L}(\mathbf{w}; \mathcal{S}) - \mathcal{L}(\mathbf{w}; \mathcal{D}). \quad (3)$$

A low generalization gap indicates a high generalization performance. Therefore, the primary objective of machine learning is to attain the optimal solution that minimizes both the training loss $\mathcal{L}(\mathbf{w}; \mathcal{S})$ and the generalization gap $\mathcal{E}(\mathbf{w})$. Although the training loss can efficiently be minimized to near zero even with a vanilla training algorithm [9], it still remains an open question how to minimize the generalization gap effectively. To address this issue, recent studies have focused on the *flatness* of the loss landscape as a potential solution [1], [10] and provided experimental evidence that a flatter loss landscape tends to have a better generalization performance [11].

Among several algorithms [4], [12], [13] that penalize sharp minima and seek flat minima, *sharpness-aware minimization* (SAM) [4] has been shown to be effective in reaching flat minima and has demonstrated significant improvements in generalization across various tasks and model structures [5], [6]. SAM aims to minimize the worst-case loss over its parameter neighborhood rather than minimizing the loss of current parameter. Let us denote a vanilla gradient descent algorithm that minimizes the loss of current weight \mathbf{w}_t at time t as

$$\mathbf{w}_{t+1} = \mathbf{w}_t - \eta \nabla \ell(\mathbf{w}_t), \quad (4)$$

where η is a learning rate and $\nabla \ell(\mathbf{v})$ is a gradient with respect to its input vector \mathbf{v} unless specified otherwise. In contrast, SAM minimizes the loss of *perturbed weight* \mathbf{w}_t^p by using the first-order Taylor approximation:

$$\mathbf{w}_t^p = \mathbf{w}_t + \rho \nabla \ell(\mathbf{w}_t). \quad (5)$$

$$\mathbf{w}_{t+1} = \mathbf{w}_t - \eta \nabla \ell(\mathbf{w}_t^p), \quad (6)$$

where ρ is a given neighborhood radius. Note that ρ can be normalized with the gradient norm as introduced in [4], i.e., $\rho / \|\nabla \ell(\mathbf{w})\|$; however, a constant ρ in (5) shows similar or higher performance than the normalized version [14]. Therefore, SAM consistently enforces \mathbf{w} to have a reduced perturbed loss $\ell(\mathbf{w}^p)$ within its ρ -neighborhood. This effectively makes the loss landscape smoother in the vicinity of its optimum, leading to a better generalization performance than that of any other existing methods.

3 RELATED WORK

3.1 Understanding Sharpness-Aware Minimization

Following the success of SAM, further investigations have been conducted to explore its algorithm and enhance its generalization performance or computational efficiency. Kwon et al. [15] proposed a transformation of parameters to achieve scale-invariant sharpness. Zhuang et al. [5] argued that subtracting $\nabla \ell(\mathbf{w})$ from $\nabla \ell(\mathbf{w}^p)$ can reduce certain drawbacks in optimization. Liu et al. [16] explored the effectiveness of a random perturbation during weight perturbation. Du et al. [17] demonstrated that perturbing only some parameters can also improve the generalization performance with a reduced computational burden.

Despite the proposed variants and their improved generalization performance, some unclear points of the mechanism behind SAM still remain. For instance, Andriushchenko et al. [14] argued that the proposed generalization bound of SAM is incomplete, and instead connected the success of SAM to its implicit bias for different sizes of mini-batch. Our work also sheds light on understanding the mechanism of SAM with respect to its optimization properties, and to the best of our knowledge, this is the first work that identifies the convergence instability near a saddle point in SAM.

3.2 Escaping Saddle Points

The non-linearity of the loss landscape of neural networks results in the presence of multiple local minima and saddle points [7], [18]. Prior studies have demonstrated that both gradient descent (GD) [7], [19] and stochastic gradient descent (SGD) [20], [21] can be hindered by the saddle point. Therefore, many researchers have focused on escaping saddle points and reaching better minima. For instance, Du et al. [7] demonstrated that GD can take exponential time to escape saddle points even when using random initialization schemes. Xie et al. [22] established SGD diffusion and the importance of momentum in overcoming the saddle point issue. Ziyin et al. [21] also demonstrated that the learning rate can affect to the saddle point escape in SGD.

Similar to these works, this study presents the difficulty of SAM in escaping the saddle point under both asymptotic and stochastic system dynamics. We introduce a dynamical

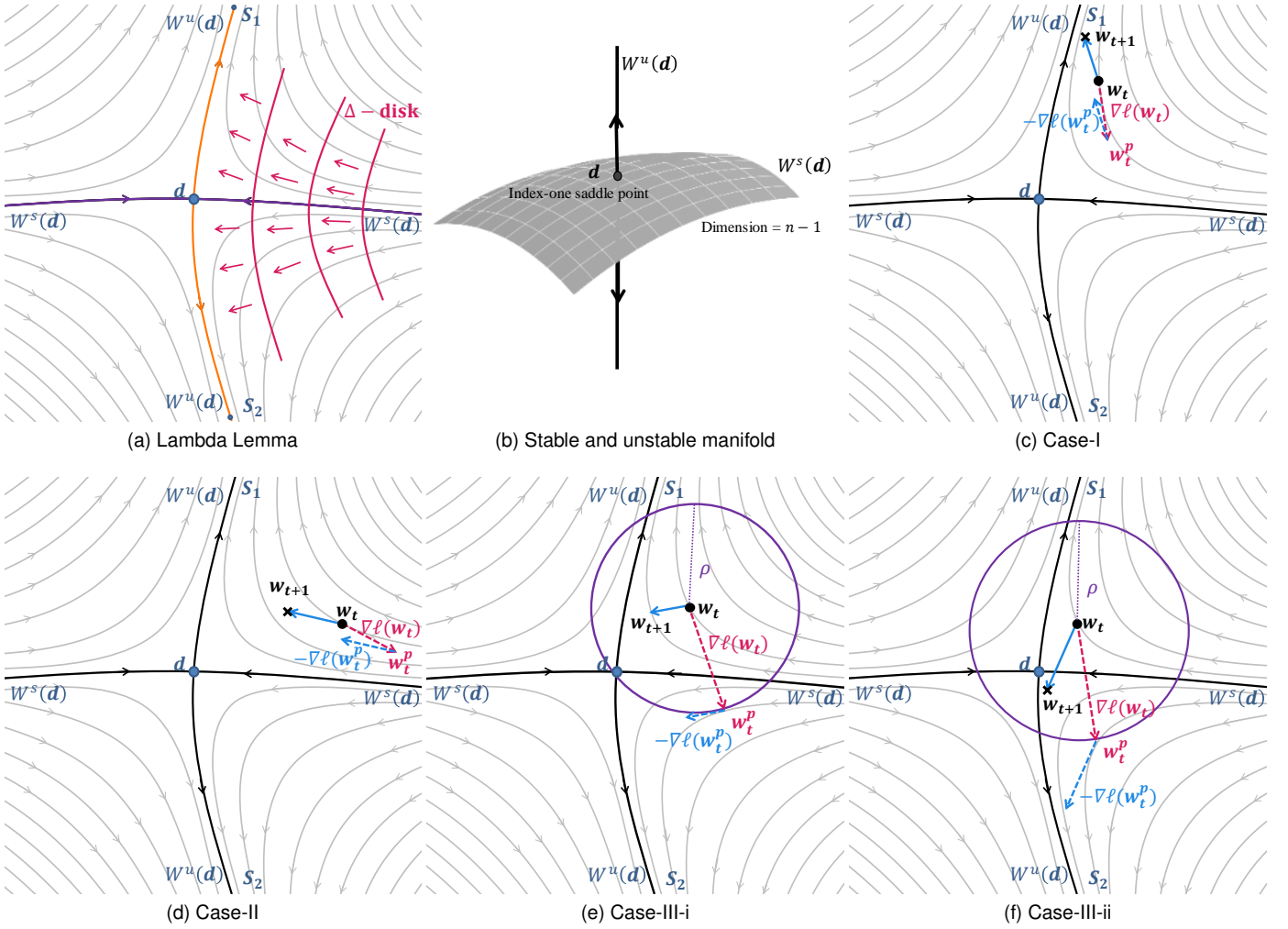


Fig. 2. (a), (b) Phase portrait of system (7) associated with the loss function ℓ . (c), (d) Phase portrait of system (7) associated with the loss function ℓ (Case-I and Case-II). (e), (f) Phase portrait of system (7) associated with the loss function ℓ (Case-III). Case-III causes the convergence instability near a saddle point.

system-based geometric method to investigate when SAM can be hindered by saddle points. Moreover, we extend the diffusion theory in SGD [22] to SAM, illustrating the convergence instability near a saddle point in SAM dynamics. Additionally, we discuss the importance of carefully adopting training tricks in SAM, which emphasizes the observation presented by [21].

4 MAIN RESULTS

In this section, we present our four main results. In Sections 4.1 to 4.2, we first investigate the mechanism of SAM in terms of a dynamical system. In Section 4.1, we illustrate the asymptotic behavior of SAM dynamics and identify the convergence instability in which SAM becomes stuck in the saddle point. In Section 4.2, we prove that a saddle point, which is not a general optimum in traditional approaches, can become an attractor in the dynamical system of SAM.

In Sections 4.3 to 4.4, we investigate the convergence instability of SAM under stochastic dynamical systems. In Section 4.3, we extend this convergence instability near a saddle point to stochastic system dynamics and further establish theoretical analyses on the difficulty of escaping

the saddle point in terms of diffusion. Finally, in Section 4.4, based on the diffusion theory, we analyze the importance of training tricks in escaping the saddle point.

4.1 Asymptotic Behavior of SAM Dynamics near Saddle Point

To investigate the underlying mechanism of SAM, we first apply a qualitative theory of dynamical systems to identify a case of convergence instability in SAM dynamics. Given the loss function $\ell(\cdot)$, we consider the following gradient flow:

$$\frac{d\mathbf{w}}{dt} = -\nabla\ell(\mathbf{w}) \quad (7)$$

We call a weight vector \mathbf{w} that satisfies $\nabla\ell(\mathbf{w}) = 0$ *equilibrium point* of system (7) and an *index- k saddle point* if its Hessian matrix $H_\ell(\mathbf{w})$ has exactly k negative eigenvalues. The *stable manifold* and the *unstable manifold* of an index- k saddle point are defined as

$$W^s(\mathbf{w}) := \{\mathbf{w}_0 : \lim_{t \rightarrow \infty} \mathbf{w}_t = \mathbf{w}\} \quad (8)$$

$$W^u(\mathbf{w}) := \{\mathbf{w}_0 : \lim_{t \rightarrow -\infty} \mathbf{w}_t = \mathbf{w}\}. \quad (9)$$

where the dimension is $n - k$ and k , respectively. Then, the *basin of attraction* of a stable (index-zero) equilibrium point s can be defined as

$$A(s) := \{w_0 : \lim_{t \rightarrow \infty} w_t = s\},$$

Its basin boundary $\partial A(s)$ consists of the (closure of) stable manifolds of index-one saddle points d_i on its boundary as

$$\partial A(s) = \bigcup_i \text{cl}(W^s(d_i)).$$

This implies that index-one saddle points d_i behave like the attractors near $\partial A(s)$.

Given the two adjacent local minima s_1 and s_2 , i.e., $\partial A(s_1) \cap \partial A(s_2)$, there exists an index-one equilibrium point d such that the 1-D unstable manifold $W^u(d)$ converges to both s_1 and s_2 with respect to system (7). Therefore, it is sufficient to consider the gradient flows near an index-one saddle point d to analyze the behavior of SAM near the basin boundary. We illustrate the basin boundaries for two adjacent local minima s_1 and s_2 and their stable and unstable manifolds in Figure 2a and Figure 2b, respectively.

To this end, we use extensively the Lambda Lemma, a key and deep theory to analyze the behavior of dynamical systems qualitatively. The Lambda Lemma in our version is stated as follows:

Lemma 1. Lambda Lemma [23], [24]. *If Δ is a 1-D disk meeting $W^s(d)$ transversely, then the gradient flows of system (7) starting from Δ arbitrarily close to $W^u(d)$.*

In other words, the gradient flows near the basin boundary but in $A(s_1)$ directs to the vector sum of $W^u(d)$ and s_1 . See Figure 2a for the illustration. Thus, the qualitative behavior of the gradient flows starting from $w_t \in A(s_1)$ falls into one of the following cases:

- **Case-I.** When w_t is “away from” an index-one saddle point d and its stable manifold $W^s(d)$: $-\nabla \ell(w_t) \sim -\nabla \ell(w_t^p)$ and w_{t+1} converges to s_1 iteratively. (See Figure 2c).
- **Case-II.** When w_t is “away from” an index-one saddle point d but near $W^s(d)$: $-\nabla \ell(w_t) \sim -\nabla \ell(w_t^p)$ and w_{t+1} approaches $W^u(d)$ by the Lambda Lemma iteratively. The subsequent weight vector update iteration will fall into the case of (I) or (III). (See Figure 2d).
- **Case-III.** When w_t is near an index-one saddle point d (i.e., $W^s(d) \cap B_\rho(w_t) \neq \emptyset$): $w_t^p \in A(s_2)$ outside of $A(s_1)$ and so $-\ell(w_t^p)$ directs to s_2 and $W^u(d)$ by the Lambda Lemma. In this case, there exist two sub-cases.
 - (i) When $w_{t+1} \in A(s_1)$: w_{t+1} approaches d and $W^s(d)$ iteratively and the subsequent weight vector update iteration will fall into the next case (ii). (See Figure 2e).
 - (ii) When $w_{t+1} \in A(s_2)$: starting from w_{t+1} , the subsequent weight vector update falls into Case-III but the roles of s_1 and s_2 are reversed. Thus, the gradient oscillates near $W^u(d)$ iteratively. (See Figure 2f).

Therefore, SAM can be hindered by the saddle point d when the perturbed weight w^p falls into a different basin of attraction across a basin boundary (Case-III), whereas GD smoothly directs to the stable equilibrium point. Furthermore, if w^p is consistently located in different basins, w_t will not be able to escape the saddle point under SAM dynamics.

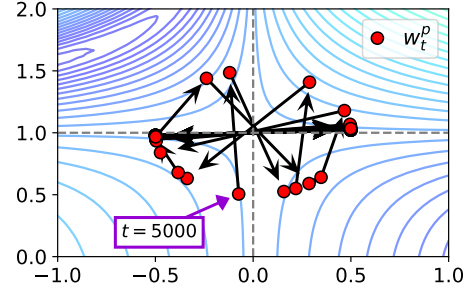


Fig. 3. Trajectory of w_t^p after the optimization step $t = 5000$, when SAM is beginning to become stuck in the saddle point during SAM optimization in Figure 1. It exhibits exactly the same behavior as that of Case-III in Figure 2.

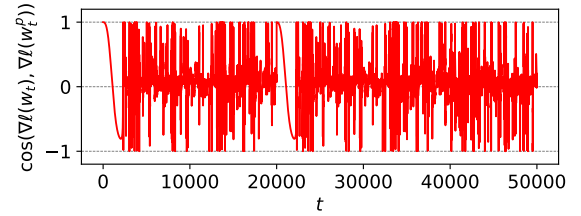


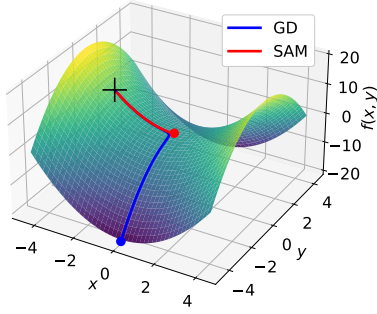
Fig. 4. Gradient oscillation during SAM optimization in Figure 1. The line corresponds to $\cos(\nabla \ell(w_t), \nabla \ell(w_t^p))$ for optimization step t . The oscillation continues until the end of the optimization.

To verify our investigation empirically, we introduce the optimization of the Beale function. This function has two benefits. First, it has a single saddle point at $(0, 1)$, which allows us to verify whether the parameter is stuck in the saddle point and the convergence instability near a saddle point. Secondly, it has four basins, as illustrated in Figure 2, with only two basins (top left and bottom right) containing a minimum. We use a learning rate of $\eta=1e-4$, as smaller learning rates often perform better on low dimensional problems. We observe similar results for other learning rates that make both GD and SAM converge.

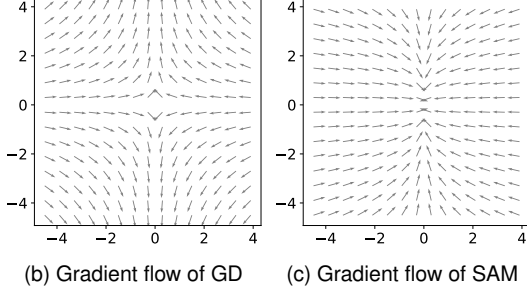
The optimization result is illustrated in Figure 1. While GD successfully converges to the global minimum, SAM is trapped in the saddle point rather than the global minimum. To verify the geometric analysis presented in Figure 2, the trajectory of the perturbed weight w_t^p is plotted in Figure 3. After SAM becomes stuck in the saddle point, w_t^p continuously crosses the basin boundaries, which is consistent with Figure 2f. Additionally, in Figure 4, the cosine between $\nabla \ell(w_t)$ and $\nabla \ell(w_t^p)$ during the optimization step t is plotted. The cosine value dramatically oscillates between -1 and 1 , which is consistent with the gradient oscillation described in Case-III-(ii). These results demonstrate that SAM becomes stuck in the saddle point as if it were a convergence point.

4.2 Saddle Point Becomes Attractor in SAM Dynamics

In the previous subsection, we observed that SAM becomes stuck in a saddle point even in the simple optimization task as if the saddle point were a convergence point. Motivated by this observation, we here mathematically derive a con-



(a) Trajectory of GD and SAM



(b) Gradient flow of GD (c) Gradient flow of SAM

Fig. 5. Optimization on $f(x, y) = x^2 - y^2$ with the saddle point at $(0, 0)$. (a) Loss surface with the initial point denoted as the plus symbol $(-3, -\epsilon)$, where $\epsilon = 0.01$. (b) Divergence of the gradient flow of GD near the saddle point. (c) Convergence of the gradient flow of SAM with $\rho = 1.0$ to the saddle point, thus making the saddle point an attractor.

dition for when a saddle point becomes an attractor under SAM dynamics as follows:

Theorem 1. Let \mathbf{d} be an index-one saddle point of system (7) with a negative eigenvalue λ_1 of the Hessian matrix $H_\ell(\mathbf{d})$ of the loss function ℓ . Then, the saddle point \mathbf{d} is an attractor of SAM dynamics in (5) if $\rho \geq -1/\lambda_1$.

Proof. See Appendix. \square

Notice that the above results can be easily generalized to any type of saddle points provided that

$$\lambda_j + \rho\lambda_j^2 \geq 0 \quad (10)$$

for all the negative eigenvalues λ_j at \mathbf{d} . Moreover, this condition is mild practically since the normalized radius $\tilde{\rho} = \rho/\|\nabla\ell(\mathbf{w})\|$ in the standard SAM dynamics [4], which becomes very large near the saddle point. This result further suggests that more points can become attractors under SAM dynamic because the term $\rho\lambda^2$ always results in positive diagonal values. Thus, Theorem 1 tells us that a saddle point can become an attractor under SAM dynamics, whereas it is not a general optimum in traditional approaches.

Figure 5 illustrates the empirical verification of Theorem 1. We perform an optimization with GD and SAM on a simple function $f(x, y) = x^2 - y^2$, which has a saddle point at $(0, 0)$. In Figure 5a, GD (blue-colored) successfully escapes the saddle point due to the benefit of a good initial point $(-3, \epsilon)$. Specifically, the gradient flow of GD (Figure 5b) demonstrates that the saddle point is not a stable equilibrium point, and thus a slight perturbation at

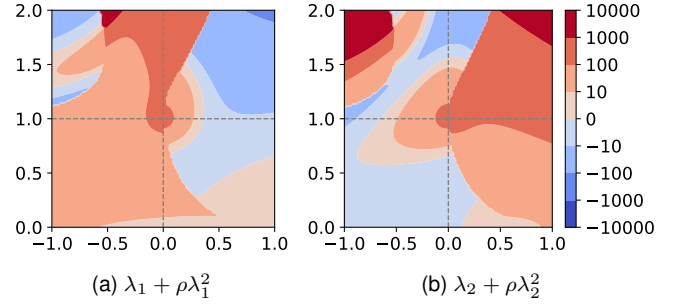


Fig. 6. Value of $\lambda + \rho\lambda^2$ for the Beale function in Figure 1. Near the saddle point at $(0, 1)$, for both eigenvalues of the Hessian, $\lambda + \rho\lambda^2$ is positive, which indicates that the saddle point becomes an attractor.

the initial point $\epsilon = 0.01$ is sufficient to help GD escape the saddle point.

In contrast, SAM becomes stuck in the saddle point (red-colored in Figure 5a). In this optimization, eigenvalues of the Hessian at $(0, 0)$ are $\lambda = \{2, -2\}$ and thus $\lambda + \rho\lambda^2 > 0$ for all eigenvalues $\lambda \in \lambda$. Therefore, by Theorem 1, the saddle point will become an attractor under SAM dynamics. The gradient flow (Figure 5c) also supports our theorem as the saddle point has now become a point of convergence, which implies that SAM will not be able to escape it.

We further explain the previous optimization result depicted in Figure 1 by calculating the eigenvalues of the Hessian for each point in the parameter space. For each point in the parameter space, we calculate the eigenvalues of the Hessian $\lambda = \{\lambda_1, \lambda_2\}$ and visualize the heat map of $\lambda + \rho\lambda^2$ in Figure 6. For both $\lambda = \lambda_1$ and λ_2 , $\lambda + \rho\lambda^2$ is positive near the saddle point, which is consistent with the behavior of the saddle point as an attractor, as illustrated in Figure 5. This suggests that the convergence instability can arise even for a more complicated loss function because the saddle point may become an attractor under SAM dynamics.

4.3 Stochastic Behavior of SAM Dynamics with Diffusion near Saddle Point

Previously, we confirmed the asymptotic behavior of SAM dynamics and its convergence instability near a saddle point. From now on, we focus on mini-batch sampling, which has been found to provide high performance in various domains [21], [25], and thus it is a commonly used technique for training deep learning models.

To investigate the behavior of SAM under stochastic system dynamics, we first establish SAM diffusion with the stochastic differential equation. Note that the basis formulations and notations are borrowed from [20], [22], [26], [27]. We assume that the perturbed weight \mathbf{w}^p is precisely calculated with (5), and thus the stochastic differential equation of SAM dynamics is formalized as follows:

$$d\mathbf{w} = -\nabla\ell(\mathbf{w}^p)dt + [\eta C(\mathbf{w}^p)]^{\frac{1}{2}}dW_t, \quad (11)$$

where η is a learning rate and $dW_t \sim \mathcal{N}(0, Idt)$ for the identity matrix I . We then draw SAM diffusion and prove that SAM escapes the saddle point more slowly than SGD.

Theorem 2. (SAM diffusion) Given a saddle point \mathbf{d} as the initial parameter under the dynamics of (11), the probability density

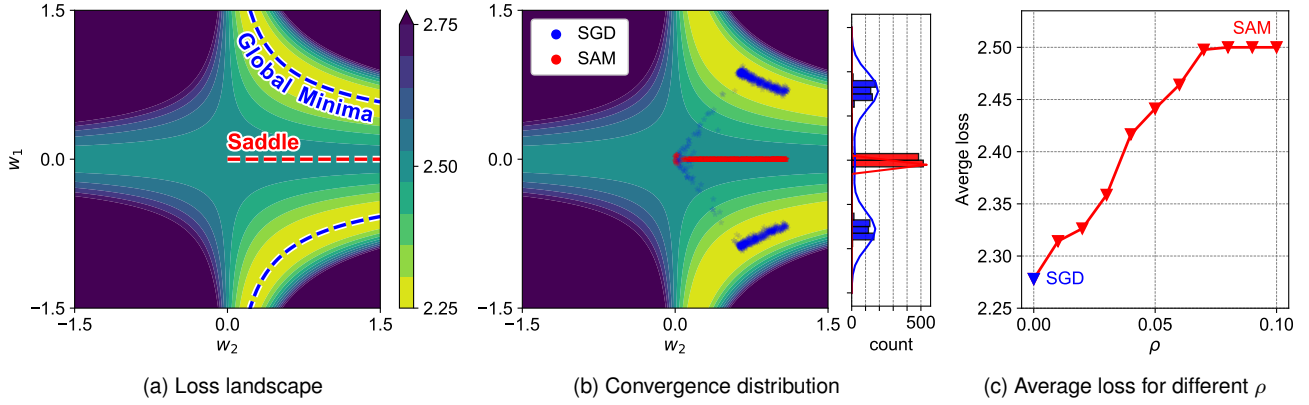


Fig. 7. Toy neural network experiment. (a) Loss landscape for different values of each neuron. (b) Distributions of converged points for SGD and SAM ($\rho = 0.1$) with the marginal distribution of the parameter w_1 . (c) Average loss of converged points for different ρ . $\rho = 0$ indicates SGD.

function of \mathbf{w} after time t is the Gaussian distribution, i.e., $\mathbf{w} \sim \mathcal{N}(\mathbf{d}, Q \text{diag}(\boldsymbol{\sigma}^2(t)) Q^T)$ with $\boldsymbol{\sigma}^2(t) = [\sigma_1^2(t), \dots, \sigma_n^2(t)]^T$, under the second-order Taylor approximation assumption near \mathbf{d} where

$$\sigma_j^2(t) = \frac{\eta |\lambda_j|}{2B \lambda_j (1 + \rho \lambda_j)^2} [1 - \exp(-2\lambda_j (1 + \rho \lambda_j)^2 t)] \quad (12)$$

for the batch size B and the j -th eigenvalue of $H(\mathbf{d})$, λ_j .

Proof. See Appendix. \square

Let us denote the mean squared displacement of the displacement $\Delta \mathbf{w}_j(t) = \mathbf{w}_j(t) - \mathbf{w}_j(0)$ by $\langle \Delta \mathbf{w}_j^2(t) \rangle$. Then, we have the following result.

Corollary 1. (SAM escapes saddle point more slowly than SGD) The mean squared displacement of SAM, denoted by $\Delta_{SGD} := \langle \Delta \mathbf{w}_j^2(t) \rangle_{SGD}$, is smaller than that of SGD, i.e., $\Delta_{SAM} := \langle \Delta \mathbf{w}_j^2(t) \rangle_{SAM}$, near the saddle point \mathbf{d} , which satisfies the following inequality:

$$\Delta_{SGD} - \Delta_{SAM} = \frac{2\eta t^2 |\lambda_j|^3}{B} \rho > 0. \quad (13)$$

Proof. See Appendix. \square

Corollary 1 tells us that SAM requires more time to escape the saddle point \mathbf{d} compared to SGD, since Δ_{SGD} is always larger than Δ_{SAM} . Furthermore, $\Delta_{SGD} - \Delta_{SAM}$ increases as ρ increases, indicating that the gap between the required time to escape the saddle point between SGD and SAM increases as ρ increases. This is also consistent with the results from Sections 4.1 and 4.2 that SAM tends to suffer convergence instability as ρ increases.

To validate our theoretical results in stochastic dynamical systems, we first conduct an experiment using a neural network and artificial settings as proposed by Ziyin et al. [21]. This experiment involves a two-layer neural network with one neuron, with a non-linear coordinate-wise activation function φ . Specifically, $\varphi(x) = x^2$ is used. The training set consists of an input x which is fixed to 1, and $y \in \{-1, 2\}$ with probability of 0.5. The loss function is the mean squared error, and thus the loss landscape yields global minima $\ell(\mathbf{w}) = 2.25$ for $\{(w_1, w_2) | w_1^2 = 1/2w_2\}$ and saddle points $\ell(\mathbf{w}) = 2.50$ for $\{(w_1, w_2) | w_1 = 0, w_2 \geq 0\}$, as illustrated in Figure 7a. Due to the presence of inherent data

uncertainty in this experiment, we can expect more practical results than those from previous experiments. Considering Theorem 2, we initialize the parameters near the saddle point, w_1 in the range $[-0.1, 0.1]$ and w_2 in the range $[0, 1]$ uniformly. Other settings remain the same as those in [21].

Figure 7b shows the converged parameter distributions for SGD and SAM over 1,000 random seeds. The results demonstrate that the converged parameters of SAM are mostly saturated in the saddle point area, whereas SGD successfully converges to the global minima. This implies that the convergence instability near a saddle point is present even in practical training settings with neural networks.

Additionally, we plot the average loss of converged points of SAM with varying ρ (Figure 7c). Here, we normalize the radius with the gradient norm during the optimization for easier comparison with prior studies [4], [5], but we observe similar results for the constant radius ρ . It is worth noting that the range of ρ in Figure 7c is commonly used in other benchmark experiments such as the CIFAR classifications [4], [5]. As ρ increases, the average loss of SAM increases. This result is in agreement with Corollary 1, as a larger ρ makes SAM more difficult to escape the saddle point in terms of diffusion, causing the convergence instability near a saddle point.

4.4 Convergence Instability and Training Tricks

The convergence instability of SAM near saddle points, which we observed under both asymptotic and stochastic dynamical systems in previous sections, can lead to suboptimal minimum problems and performance degradation [7], [8], [21]. However, this is in contradiction to the claims of prior studies [4], [5], which state that SAM and its variants generally perform better than other methods on various benchmark datasets. In this section, we theoretically and empirically demonstrate that often used training tricks, such as momentum and batch size, not only help SAM to escape the saddle point but are also the key to its success.

First, we extend SAM diffusion presented in Theorem 2 to include momentum and investigate the relationship between the mean squared displacement of SAM, momentum, and batch size.

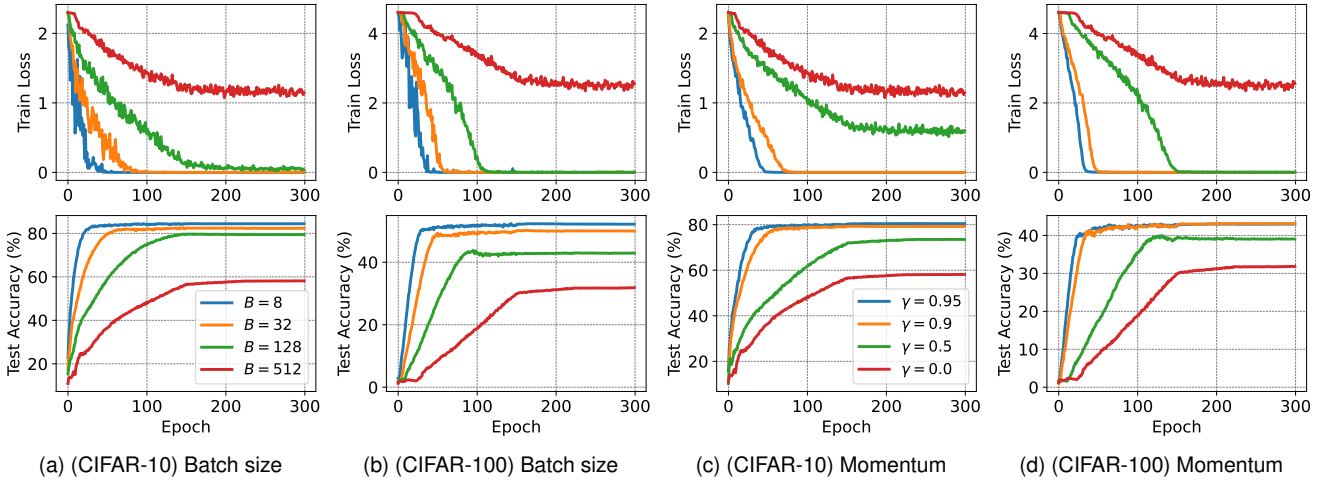


Fig. 8. Effect of varying batch size B and momentum γ . To measure the pure effect of batch size and momentum, batch normalization and data augmentation are turned off. A smaller batch size and larger momentum lead to better performance of SAM.

Theorem 3. (SAM diffusion, momentum, and batch size)

Given a momentum hyper-parameter γ and batch size B , the mean squared displacement of SAM is given by

$$\Delta_{SAM} = C_1 \frac{(1 - e^{-C_2(1-\gamma)})^2}{(1-\gamma)^3 B} + C_3 \frac{(1 - e^{-\frac{C_4}{1-\gamma}})}{(1-\gamma)B}, \quad (14)$$

where $C_1 = \frac{\eta^2 |\lambda_j|}{2}$, $C_2 = \frac{\eta}{t}$, $C_3 = \frac{\eta |\lambda_j|}{2\lambda_j(1+\rho\lambda_j)^2}$, and $C_4 = 2\lambda_j(1+\rho\lambda_j)^2 t$ are positive constants and λ_j denotes eigenvalue of the Hessian matrix $H_\ell(\mathbf{d})$ of loss function ℓ at saddle point \mathbf{d} . Therefore, Δ_{SAM} increases as (1) momentum increases and/or (2) batch size decreases. Furthermore, as $(1-\gamma)B \rightarrow 0$, we have

$$\Delta_{SAM} \propto \frac{1}{(1-\gamma)B}. \quad (15)$$

Proof. See Appendix. \square

Theorem 3 tells us that increasing momentum γ and decreasing batch size B can reduce the time to escape a saddle point. This result is consistent with the work of Andriushchenko et al. [14], which observed that a smaller batch size significantly increases the performance of SAM. While we derived the advantage of small batch size from the diffusion term, Andriushchenko et al. [14] provided theoretical proof of the benefit of a small batch size from the concept of implicit bias. Integrating these theoretical analyses might be possible, but we leave it as future work.

To empirically verify Theorem 3, we evaluate the effects of momentum and batch size on the commonly used benchmarks, CIFAR-10 and CIFAR-100. To compare the pure effect of momentum and batch size, we turn off both batch normalization and data augmentation. We fix the radius $\rho = 0.1$ and use the momentum $\gamma = 0.0$ and batch size $B = 512$ as default, and then vary the batch size and momentum independently. We normalize the radius with the gradient norm during the training phase as same as in the previous subsection, but we observe similar results for the constant radius ρ similar to [14]. All the models are trained for 300 epochs to ensure the convergence.

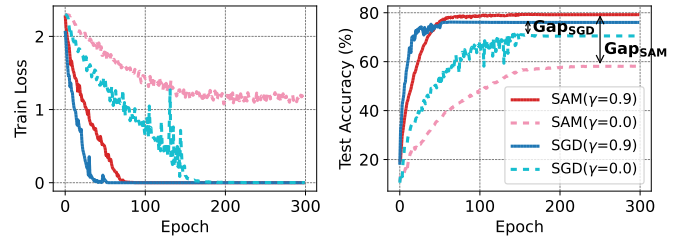


Fig. 9. (CIFAR-10) Effect of momentum γ for SGD and SAM. Batch normalization and data augmentation are turned off. The momentum increases more dramatically the performance of SAM compared to that of SGD.

Figure 8 provides a summary of the training loss and test accuracy for each batch size and momentum. Figures 8a and 8b demonstrate that SAM struggles to minimize the training loss as the batch size increases. Notably, for a batch size of $B = 512$, SAM displays convergence instability with the train loss exceeding 1, which results in a poor generalization performance of less than 60% accuracy.

In addition, momentum has a significant impact on the training loss and test accuracy (Figures 8c and 8d). As momentum increases, the test accuracy increase. This effect is particularly pronounced when compared to that on SGD. Figure 9 shows the train loss and test accuracy for SAM and SGD with $\gamma = 0.0$ and 0.9 . The momentum improves the accuracy of SGD by approximately 5%, whereas it enhances the accuracy of SAM by more than 20%.

Considering Corollary 1, Figure 9 implies that a higher momentum could be beneficial for SAM as ρ increases. We evaluate the test accuracy of SAM for different radius ρ and momentum γ . Here, to obtain their best performance, we turn on batch normalization and data augmentation. Table 1 shows the average and standard deviation of test accuracy over three different random seeds. The minimum accuracies are observed only for $\gamma = 0.0$, whereas the best performance is observed for $\gamma = 0.9$ or 0.95 . Furthermore, as ρ increases, the gap between the best and worst performances increases, and a higher momentum yields better performance. Con-

TABLE 1

(CIFAR-10) Test accuracy for different momentum γ and radius ρ . The bold and underlined numbers denote the maximum and minimum accuracy for each ρ , respectively. Batch normalization and data augmentation are turned on.

SAM Radius ρ	Momentum γ			Gap (Max - Min)
	0.0	0.9	0.95	
0.01	93.77±0.08	94.99±0.09	94.94±0.09	1.22
0.05	<u>93.56±0.03</u>	95.01±0.11	94.94±0.11	1.45
0.1	<u>92.29±0.08</u>	94.84±0.15	95.08±0.07	2.80
0.5	<u>86.20±1.66</u>	88.76±1.14	91.98±0.03	5.79

sidering the fact that $\rho = 0.1$ with $\gamma = 0.95$ yields the best accuracy over all combinations, using a higher momentum with a larger ρ can be beneficial to improve the generalization performance under SAM dynamics.

5 CONCLUSION

To gain insight into SAM dynamics, we analyzed its convergence instability near a saddle point. Through theoretical and empirical analyses, we demonstrated that this convergence problem can occur in various tasks, from a simple optimization to complicated neural network training. Additionally, we demonstrated the importance of momentum and batch size in relation to the diffusion theory. We believe that our work sheds light on understanding the mechanism of SAM and hope that future work will build upon our findings to develop new training methods.

REFERENCES

- [1] S. Hochreiter and J. Schmidhuber, "Simplifying neural nets by discovering flat minima," *Advances in neural information processing systems*, vol. 7, 1994.
- [2] N. S. Keskar, J. Nocedal, P. T. P. Tang, D. Mudigere, and M. Smelyanskiy, "On large-batch training for deep learning: Generalization gap and sharp minima," in *5th International Conference on Learning Representations, ICLR 2017*, 2017.
- [3] H. Li, Z. Xu, G. Taylor, C. Studer, and T. Goldstein, "Visualizing the loss landscape of neural nets," *Advances in neural information processing systems*, vol. 31, 2018.
- [4] P. Foret, A. Kleiner, H. Mobahi, and B. Neyshabur, "Sharpness-aware minimization for efficiently improving generalization," in *International Conference on Learning Representations*, 2020.
- [5] J. Zhuang, B. Gong, L. Yuan, Y. Cui, H. Adam, N. C. Dvornek, J. s Duncan, T. Liu *et al.*, "Surrogate gap minimization improves sharpness-aware training," in *International Conference on Learning Representations*, 2021.
- [6] X. Chen, C.-J. Hsieh, and B. Gong, "When vision transformers outperform resnets without pre-training or strong data augmentations," in *International Conference on Learning Representations*, 2022. [Online]. Available: <https://openreview.net/forum?id=LtKcMgGOeLt>
- [7] S. S. Du, C. Jin, J. D. Lee, M. I. Jordan, A. Singh, and B. Póczos, "Gradient descent can take exponential time to escape saddle points," *Advances in neural information processing systems*, vol. 30, 2017.
- [8] B. Kleinberg, Y. Li, and Y. Yuan, "An alternative view: When does sgd escape local minima?" in *International Conference on Machine Learning*. PMLR, 2018, pp. 2698–2707.
- [9] T. Ishida, I. Yamane, T. Sakai, G. Niu, and M. Sugiyama, "Do we need zero training loss after achieving zero training error?" in *International Conference on Machine Learning*. PMLR, 2020, pp. 4604–4614.
- [10] G. K. Dziugaite and D. M. Roy, "Computing nonvacuous generalization bounds for deep (stochastic) neural networks with many more parameters than training data," *arXiv preprint arXiv:1703.11008*, 2017.
- [11] Y. Jiang, B. Neyshabur, H. Mobahi, D. Krishnan, and S. Bengio, "Fantastic generalization measures and where to find them," in *International Conference on Learning Representations*, 2019.
- [12] P. Chaudhari, A. Choromanska, S. Soatto, Y. LeCun, C. Baldassi, C. Borgs, J. Chayes, L. Sagun, and R. Zecchina, "Entropy-sgd: Biasing gradient descent into wide valleys," *Journal of Statistical Mechanics: Theory and Experiment*, vol. 2019, no. 12, p. 124018, 2019.
- [13] P. Izmailov, A. Wilson, D. Podoprikin, D. Vetrov, and T. Garipov, "Averaging weights leads to wider optima and better generalization," in *34th Conference on Uncertainty in Artificial Intelligence 2018, UAI 2018*, 2018, pp. 876–885.
- [14] M. Andriushchenko and N. Flammarion, "Towards understanding sharpness-aware minimization," in *International Conference on Machine Learning*. PMLR, 2022, pp. 639–668.
- [15] J. Kwon, J. Kim, H. Park, and I. K. Choi, "Asam: Adaptive sharpness-aware minimization for scale-invariant learning of deep neural networks," in *International Conference on Machine Learning*. PMLR, 2021, pp. 5905–5914.
- [16] Y. Liu, S. Mai, M. Cheng, X. Chen, C.-J. Hsieh, and Y. You, "Random sharpness-aware minimization," in *Advances in Neural Information Processing Systems*, A. H. Oh, A. Agarwal, D. Belgrave, and K. Cho, Eds., 2022. [Online]. Available: <https://openreview.net/forum?id=htUvh7xPoa>
- [17] J. Du, H. Yan, J. Feng, J. T. Zhou, L. Zhen, R. S. M. Goh, and V. Tan, "Efficient sharpness-aware minimization for improved training of neural networks," in *International Conference on Learning Representations*, 2022. [Online]. Available: <https://openreview.net/forum?id=n0OeTdNRG0Q>
- [18] B. Kleinberg, Y. Li, and Y. Yuan, "An alternative view: When does SGD escape local minima?" in *Proceedings of the 35th International Conference on Machine Learning*, ser. Proceedings of Machine Learning Research, J. Dy and A. Krause, Eds., vol. 80. PMLR, 10–15 Jul 2018, pp. 2698–2707.
- [19] J. D. Lee, M. Simchowitz, M. I. Jordan, and B. Recht, "Gradient descent only converges to minimizers," in *Conference on learning theory*. PMLR, 2016, pp. 1246–1257.
- [20] Z. Xie, I. Sato, and M. Sugiyama, "A diffusion theory for deep learning dynamics: Stochastic gradient descent exponentially favors flat minima," in *International Conference on Learning Representations*, 2020.
- [21] L. Ziyin, B. Li, J. B. Simon, and M. Ueda, "SGD can converge to local maxima," in *International Conference on Learning Representations*, 2022. [Online]. Available: <https://openreview.net/forum?id=9XhPLAjjRB>
- [22] Z. Xie, X. Wang, H. Zhang, I. Sato, and M. Sugiyama, "Adaptive inertia: Disentangling the effects of adaptive learning rate and momentum," in *International Conference on Machine Learning*. PMLR, 2022, pp. 24 430–24 459.
- [23] J. Guckenheimer and P. Holmes, *Nonlinear oscillations, dynamical systems, and bifurcations of vector fields*. Springer Science & Business Media, 2013, vol. 42.
- [24] J. J. Palis and W. De Melo, *Geometric theory of dynamical systems: an introduction*. Springer Science & Business Media, 2012.
- [25] E. Hoffer, I. Hubara, and D. Soudry, "Train longer, generalize better: closing the generalization gap in large batch training of neural networks," *Advances in neural information processing systems*, vol. 30, 2017.
- [26] H. Risken, "Fokker-planck equation," in *The Fokker-Planck Equation*. Springer, 1996, pp. 63–95.
- [27] I. Sato and H. Nakagawa, "Approximation analysis of stochastic gradient langevin dynamics by using fokker-planck equation and its process," in *International Conference on Machine Learning*. PMLR, 2014, pp. 982–990.
- [28] S. Mandt, M. D. Hoffman, and D. M. Blei, "Stochastic gradient descent as approximate bayesian inference," *arXiv preprint arXiv:1704.04289*, 2017.
- [29] Y. Pawitan, *In all likelihood: statistical modelling and inference using likelihood*. Oxford University Press, 2001.
- [30] S. Jastrzkebski, Z. Kenton, D. Arpit, N. Ballas, A. Fischer, Y. Bengio, and A. Storkey, "Three factors influencing minima in sgd," *arXiv preprint arXiv:1711.04623*, 2017.
- [31] Z. Zhu, J. Wu, B. Yu, L. Wu, and J. Ma, "The anisotropic noise in stochastic gradient descent: Its behavior of escaping from sharp minima and regularization effects," *arXiv preprint arXiv:1803.00195*, 2018.

SUPPLEMENTS TO STABILITY ANALYSIS OF SHARPNESS-AWARE MINIMIZATION

Without loss of generality, we assume that (7) is *hyperbolic* so that the Hessian matrix of ℓ at each equilibrium point has no zero eigenvalues, which is a generic property that holds for typical loss functions. Then, the Hessian matrix has real eigenvalues because it is a real symmetric matrix.

Proofs

Proof of Theorem 1

Proof. Given the gradient flow of SAM in (5), we have

$$\frac{d\mathbf{w}}{dt} = -\nabla\ell(\mathbf{w} + \rho\nabla\ell(\mathbf{w})) \quad (16)$$

$$\frac{d^2\mathbf{w}}{dt^2} = -\nabla^2\ell(\mathbf{w} + \rho\nabla\ell(\mathbf{w}))[I + \rho\nabla^2\ell(\mathbf{w})]. \quad (17)$$

Since the Hessian matrix is a real symmetric matrix, $H_\ell(\mathbf{d}) = Q\Lambda Q^T$, where Q is a real orthogonal matrix and $\Lambda = \mathbf{diag}[\lambda_1, \dots, \lambda_n]^T$ is a real diagonal matrix consisting of eigenvalues as its elements. Given a saddle point \mathbf{d} , we have $\nabla\ell(\mathbf{d}) = 0$ and thus (17) becomes

$$\left. \frac{d^2\mathbf{w}}{dt^2} \right|_{\mathbf{w}=\mathbf{d}} = -\nabla^2\ell(\mathbf{d} + \rho\nabla\ell(\mathbf{d}))[I + \rho\nabla^2\ell(\mathbf{d})] \quad (18)$$

$$= -Q(\Lambda + \rho\Lambda^2)Q^T. \quad (19)$$

As all the diagonal elements of $\Lambda + \rho\Lambda^2$ are positive, \mathbf{d} becomes an attractor of SAM dynamics. \square

Under the dynamics of (11), we use the Fokker-Planck equation that describes the probability density of the weight \mathbf{w} as follows [20]:

$$\frac{\partial P(\mathbf{w}, t)}{\partial t} = \nabla \cdot [P(\mathbf{w}, t)\nabla\ell(\mathbf{w}^p)] + \nabla \cdot \nabla[D(\mathbf{w}^p)P(\mathbf{w}, t)]. \quad (20)$$

where $\nabla \cdot$ is the divergence operator and the diffusion matrix is given by

$$D(\mathbf{w}^p) = \frac{\eta C(\mathbf{w}^p)}{2}, \quad (21)$$

Now, we assume the following **second-order Taylor approximation** of the loss function ℓ near saddle points \mathbf{d} , which holds locally around critical points and is commonly adopted in [20], [22], [28]:

$$\ell(\mathbf{w}) = \ell(\mathbf{d}) + \frac{1}{2}(\mathbf{w} - \mathbf{d})^T H_\ell(\mathbf{d})(\mathbf{w} - \mathbf{d}).$$

Proof of Theorem 2

Proof. The solution of the Fokker-Planck Equation (20) should be formalized as follows:

$$P(\mathbf{w}, t) = \left(\prod_{j=1}^n 2\pi\sigma_j \right)^{-\frac{1}{2}} \exp \left(-\frac{1}{2}(\mathbf{w} - \mathbf{d})^T Q \mathbf{diag}(\boldsymbol{\sigma}^2(t)) Q^T (\mathbf{w} - \mathbf{d}) \right). \quad (22)$$

To be self-contained, we mainly followed Appendix A.1 in [22]. Let us denote the loss function of the i -th training sample $\ell_i(\mathbf{w})$ among N samples in total. By using the Fisher Information Matrix (FIM) [29], the following approximation can be adopted near the critical point \mathbf{d} as described in [22], [30], [31].

$$C(\mathbf{w}) \approx \frac{1}{B} \left[\frac{1}{N} \sum_{i=1}^N \nabla\ell_i(\mathbf{w})\nabla\ell_i(\mathbf{w})^T \right] = \frac{1}{B} \text{FIM}(\mathbf{w}) \approx \frac{1}{B} [H(\mathbf{w})]^+. \quad (23)$$

Here, given $A = V \mathbf{diag}([\lambda_1, \dots, \lambda_n]^T) V^T$, we denote $V \mathbf{diag}([\lambda_1, \dots, \lambda_n]^T) V^T$ as $[A]^+$. By the above equation and Assumption 5, near the critical point, $D(\mathbf{w})$ is independent of \mathbf{w} , i.e.,

$$D = \frac{\eta}{2B} [H]^+. \quad (24)$$

where $H(\mathbf{d}) = H$ for simplicity.

Following [22], without loss of generality, we consider one-dimensional solution. Under the second-order Taylor approximation assumption, we have

$$\begin{aligned} \nabla\ell(\mathbf{w}^p) &= \nabla \left[\ell(\mathbf{d}) + \frac{1}{2}(\mathbf{w}^p - \mathbf{d})^T H(\mathbf{w}^p - \mathbf{d}) \right] \\ &= H[\mathbf{w} + \rho\nabla\ell(\mathbf{w})]\nabla[\mathbf{w} + \rho\nabla\ell(\mathbf{w})] = H[I + \rho H]^2 \mathbf{w}. \end{aligned}$$

Then, the right term of (20) can be formalized as

$$\begin{aligned}\nabla \cdot [P(\mathbf{w}, t) \nabla \ell(\mathbf{w}^p)] + \nabla \cdot \nabla [D(\mathbf{w}^p) P(\mathbf{w}, t)] &= P(\mathbf{w}, t) H[I + \rho H]^2 - H[I + \rho H]^2 \cdot \frac{\mathbf{w}}{\sigma^2} P(\mathbf{w}, t) + D \left(\frac{\mathbf{w}^2}{\sigma^4} - \frac{1}{\sigma^2} \right) P(\mathbf{w}, t) \\ &= \left(1 - \frac{\mathbf{w}^2}{\sigma^2} \right) H[I + \rho H]^2 P(\mathbf{w}, t) + D \left(\frac{\mathbf{w}^2}{\sigma^4} - \frac{1}{\sigma^2} \right) P(\mathbf{w}, t) \\ &= (-\sigma^2 H[I + \rho H]^2 + D) \left(\frac{\mathbf{w}^2}{\sigma^4} - \frac{1}{\sigma^2} \right) P(\mathbf{w}, t).\end{aligned}$$

On the other hand, the left term of (20) can be formalized as

$$\frac{\partial P(\mathbf{w}, t)}{\partial t} = \frac{1}{2} \left(\frac{\mathbf{w}^2}{\sigma^4} - \frac{1}{\sigma^2} \right) P(\mathbf{w}, t) \frac{\partial \sigma^2}{\partial t}.$$

Thus, the solution of (20) is

$$\frac{\partial \sigma^2}{\partial t} = 2D - 2\sigma^2 H[I + \rho H]^2,$$

By using the initial condition $\sigma^2(0) = 0$ and (24), we can obtain

$$\sigma_j^2(t) = \frac{\eta |\lambda_j|}{2B\lambda_j(1 + \rho\lambda_j)^2} [1 - \exp(-2\lambda_j(1 + \rho\lambda_j)^2 t)].$$

□

Proof of Corollary 1

Proof. By the definition of the mean squared displacement, $\langle \Delta \mathbf{w}_j^2(t) \rangle$ is equal to $\overline{\sigma_j^2(t)}$. Thus, given Theorem 2,

$$\begin{aligned}\Delta_{SGD} &= \frac{\eta |\lambda_j|}{2B\lambda_j} [1 - \exp(-2\lambda_j t)] \\ \Delta_{SAM} &= \frac{\eta |\lambda_j|}{2B\lambda_j(1 + \rho\lambda_j)^2} [1 - \exp(-2\lambda_j(1 + \rho\lambda_j)^2 t)].\end{aligned}$$

As $|\lambda_j|t \ll 1$ near ill-conditioned saddle points [22], the difference $\Delta_{SGD} - \Delta_{SAM}$ can be formalized as follows:

$$\begin{aligned}\Delta_{SGD} - \Delta_{SAM} &\approx \frac{\eta |\lambda_j|}{2B\lambda_j(1 + \rho\lambda_j)^2} [(1 + \rho\lambda_j)^2 [2\lambda_j t - 2(\lambda_j t)^2] - [2\lambda_j(1 + \rho\lambda_j)^2 t - 2(\lambda_j(1 + \rho\lambda_j)^2 t)^2]] \\ &= \frac{\eta \lambda_j |\lambda_j|}{B} [(t + \rho\lambda_j t)^2 - t^2] = \frac{\eta \lambda_j |\lambda_j|}{B} [2\rho\lambda_j t^2 + (\rho\lambda_j t)^2] \\ &\approx \frac{2\eta t^2 |\lambda_j|^3 \rho}{B}.\end{aligned}$$

□

Proof of Theorem 3

Proof. Similar to Theorem 2, we consider the on-dimensional case near a critical point. As the momentum dynamics with a momentum γ and dampening τ can be written as follows:

$$\begin{aligned}\mathbf{m}_t &= \gamma \mathbf{m}_{t-1} + (1 - \tau) \mathbf{g}_t \\ \mathbf{w}_{t+1} &= \mathbf{w}_t - \eta \mathbf{m}_t\end{aligned}$$

We let $dt = \eta$, $\phi = \frac{1-\gamma}{dt}$, and $M = \frac{dt}{1-\tau}$. Then, the stochastic differential equation and its Fokker-Planck Equation becomes

$$\begin{aligned}M d\dot{\mathbf{w}} &= -\phi d\mathbf{w} - \frac{\partial \ell(\mathbf{w})}{\partial \mathbf{w}} dt + [2D]^{1/2} dW_t \\ \frac{\partial P(\mathbf{w}, \mathbf{b}, t)}{\partial t} &= -\nabla_{\mathbf{w}} \cdot [\mathbf{b} P(\mathbf{w}, \mathbf{b}, t)] + \nabla_{\mathbf{b}} [\phi \mathbf{m} + M^{-1} \nabla_{\mathbf{w}} \ell(\mathbf{w})] P(\mathbf{w}, \mathbf{b}, t) + \nabla_{\mathbf{b}} \cdot M^{-2} D \cdot \nabla_{\mathbf{b}} P(\mathbf{w}, \mathbf{b}, t).\end{aligned}$$

where $\dot{\mathbf{w}} := \frac{d\mathbf{w}}{dt}$. Further, combining the proof of Theorem 2 in [22] and Theorem 2 in the main paper, we have the mean squared displacement of SAM with ρ for dampening $\tau = 0$,

$$\begin{aligned}\langle \Delta \mathbf{w}_j^2(t) \rangle &= \frac{\eta |\lambda_j|}{2\phi^3 M^2 B} [1 - \exp(-\phi t)]^2 + \frac{\eta |\lambda_j|}{2\phi M B \lambda_j (1 + \rho\lambda_j)^2} \left[1 - \exp\left(-\frac{2\lambda_j(1 + \rho\lambda_j)^2 t}{\phi M}\right) \right] \\ &= \frac{\eta^2 |\lambda_j|}{2(1 - \gamma)^3 B} \left[1 - \exp\left(-\frac{1 - \gamma}{\eta} t\right) \right]^2 + \frac{\eta |\lambda_j|}{2(1 - \gamma) B \lambda_j (1 + \rho\lambda_j)^2} \left[1 - \exp\left(-\frac{2\lambda_j(1 + \rho\lambda_j)^2 t}{1 - \gamma}\right) \right].\end{aligned}$$

Let $C_1 = \frac{\eta^2 |\lambda_j|}{2}$, $C_2 = \frac{\eta}{t}$, $C_3 = \frac{\eta |\lambda_j|}{2\lambda_j(1+\rho\lambda_j)^2}$, and $C_4 = 2\lambda_j(1+\rho\lambda_j)^2 t$. Note that C_1, C_2, C_3 , and C_4 are positive. The above equation can be reformulated as follows:

$$\langle \Delta \mathbf{w}_j^2(t) \rangle = \frac{C_1}{(1-\gamma)^3 B} [1 - \exp(-C_2(1-\gamma))]^2 + \frac{C_3}{(1-\gamma)B} \left[1 - \exp\left(-\frac{C_4}{1-\gamma}\right) \right].$$

The second term in the right-hand side is an increasing function with respect to $\gamma \in [0, 1]$, since both $\frac{C_3}{(1-\gamma)}$ and $1 - \exp\left(-\frac{C_4}{1-\gamma}\right)$ are increasing functions with respect to γ . For the first term in the right-hand, we use the following function.

$$h(\gamma) = \frac{1}{(1-\gamma)^3} \left[1 - e^{-C_2(1-\gamma)} \right]^2.$$

We have $h(0) = (1 - e^{-C_2})^2 > 0$ and

$$h'(\gamma) = \frac{e^{-2C_2(1-\gamma)} [e^{C_2(1-\gamma)} - 1]}{(1-\gamma)^4} \left[3(e^{C_2(1-\gamma)} - 1) - 2C_2(1-\gamma) \right] > 0,$$

since $e^{C_2(1-\gamma)} - 1 \geq C_2(1-\gamma)$ for $\gamma \in [0, 1]$ and $C_2 > 0$. Therefore, $h(\gamma)$ is an increasing function with respect to $\gamma \in [0, 1]$. Thus, $\langle \Delta \mathbf{w}_j^2(t) \rangle$ is also an increasing function with respect to γ . Furthermore, as $(1-\gamma)B \rightarrow 0$, we have

$$\begin{aligned} \Delta_{SAM} &\approx \frac{C_1}{(1-\gamma)^3 B} [1 - (1 - C_2(1-\gamma))]^2 + \frac{C_3}{(1-\gamma)B} \left[1 - \left(1 - \frac{C_4}{1-\gamma}\right) \right] \\ &\approx \frac{C_1 C_2^2 (1-\gamma)^2}{(1-\gamma)^3 B} + \frac{C_3}{(1-\gamma)B} = \frac{C_1 C_2^2 + C_3}{(1-\gamma)B} \propto \frac{1}{(1-\gamma)B}. \end{aligned}$$

□